Comparing sound radiation from a loudspeaker with that from a flexible spherical cap on a rigid sphere*

Ronald M. Aarts[1,2], *AES fellow*, and Augustus J.E.M. Janssen[2,3]

[1]Philips Research Laboratories,
HTC 36, 5656 AE Eindhoven, The Netherlands
[2]Eindhoven University of Technology, Department of Electrical Engineering,
Den Dolech 2, 5600 MB Eindhoven, The Netherlands
[3]Eindhoven University of Technology, EURANDOM,
Den Dolech 2, 5600 MB Eindhoven, The Netherlands

December 23, 2010

Abstract

It has been suggested by Morse and Ingard that the sound radiation of a loudspeaker in a box is comparable with that of a spherical cap on a rigid sphere. This has been established recently by the authors of this paper who have developed a computation scheme for the forward and inverse calculation of the pressure due to a harmonically excited, flexible cap on a rigid sphere with an axially symmetric velocity distribution. In this paper, the comparison is done for other quantities that are relevant for audio engineers, viz. the baffle-step response, sound power and directivity, and the acoustic center of the radiator.

0 Introduction

The sound radiation of a loudspeaker is often modeled by assuming the loudspeaker cabinet to be a rigid infinite baffle around a circularly symmetric membrane. Given a velocity distribution on the membrane, the pressure in front of the baffle due to a harmonic excitation is then described by Rayleigh's integral [1] or by King's integral [2]. The theory for this model has been

*This paper is partly based on paper 7989 presented at the 128th Convention 2010 May 22–25 London, UK.

firmly established, both analytically and computationally, in many journal papers [3, 4, 5, 6, 7, 8, 9, 10] and textbooks [11, 12, 13, 14]. The results thus obtained are in good correspondence with what one obtains when the loudspeaker is modeled as being a finite-extent box-like cabinet with a circular, vibrating membrane [15, 16]. Here one should, however, restrict to the region in front of the loudspeaker and not too far from the axis. The validity of the infinite-baffle model becomes questionable, or even nonsensical, on the side region or behind the loudspeaker [12, p. 181].

It has been suggested by Morse and Ingard [11, Sec. 7.2], that using a sphere with a membrane on a spherical cap as a simplified model of a loudspeaker whose cabinet has roughly the same width, height and depth, produces comparable results as the true loudspeaker. An application for the cap model is that it can be used to predict the polar behavior of a loudspeaker cabinet. Pressure calculations for true loudspeakers can normally only be done by using advanced numerical techniques [15, 16]. In the case of the spherical-cap model, the pressure can be computed as the the solution of the Helmholtz equation with spherical boundary conditions in the form of series involving the products of spherical harmonics and spherical Hankel functions [17, Ch. 11.3], [18, Ch. III, Sec. 6], [11, Ch. 7], [19, Ch. 19–21] using coefficients that are determined from the boundary conditions at the sphere including the flexible cap. In [20] there is a discussion on how the polar cap model for sphere radius $R \to \infty$ agrees with the model that uses the flat piston in an infinite baffle. When the cap aperture angle θ_0 approaches π, the solution becomes that of the simple pulsating sphere. Hence, the polar cap solution subsumes the solutions of the two classic radiation problems. This very same issue, for the case of a piston, has been addressed by Rogers and Williams [21]. In [22] the spherical-cap model has been used to describe sound radiation from a horn.

In [23] the authors of the present paper make a detailed comparison, on the level of polar plots, of the pressure (SPL) due to a true loudspeaker and the pressure computed using the spherical-cap model. The standard computation scheme for this model has been modified in [23] in the interest of solving the inverse problem of estimating the velocity distribution on the membrane from measured pressure data around the sphere. To accommodate the stability of the solution of this inverse problem, an efficient parametrization of velocity profiles vanishing outside the cap in terms of expansion coefficients with respect to orthogonal functions on the cap is used. This leads to a more complicated computation scheme than the standard one, with the advantage that it can be used in both forward and reversed direction. The emphasizes in the present paper is on comparing acoustical quantities that can be obtained from the spherical-cap model by forward computation, and so the more complicated scheme in [23] is not needed. Hence the standard scheme is used in the present paper.

The quantities considered in this paper for comparing the results from a true loudspeaker and those produced by using the spherical cap are:

- the baffle step response,
- sound power and directivity,

- the acoustic center.

In Sec. 1 the geometry and a detailed overview of the basic formulas and some results of [23] are given. In Sec. 2 the baffle-step response computed using the spherical-cap model and the one obtained from the loudspeaker are compared. In Sec. 3 the same is done for the sound power and directivity, while in Sec. 4 the acoustic center is considered. In Sec. 5 the conclusions and outlook for further work are presented.

1 Geometry and basic formulas

Assume an axisymmetric velocity profile $V(\theta)$, in normal direction on a spherical cap S_0 given in spherical coordinates as

$$S_0 = \{(r, \theta, \varphi) \mid r = R\,,\ 0 \le \theta \le \theta_0\,,\ 0 \le \varphi \le 2\pi\}\,, \tag{1}$$

with R the radius of the sphere with center at the origin and θ_0 the aperture angle of the cap measured from the center. The half-line $\theta = 0$ is identified with the positive z-direction in the Cartesian coordinate system, see Fig. 1 for the used geometry and notations. It is assumed that V vanishes outside

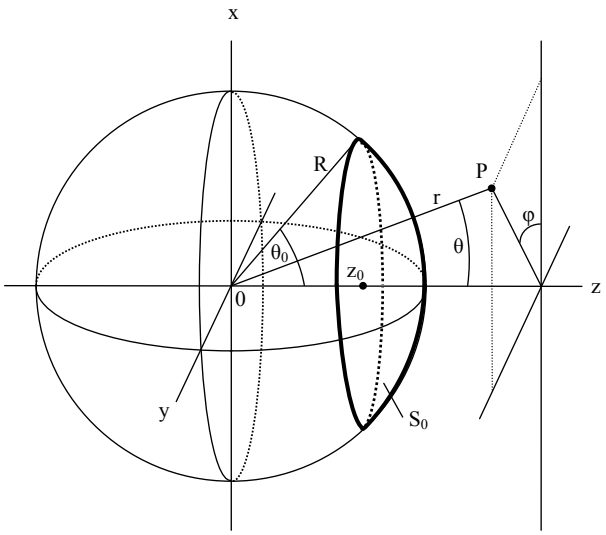

Figure 1: Geometry and notations.

S_0. Furthermore, as is commonly the case in loudspeaker applications, the cap moves parallel to the z-axis, according to the component

$$W(\theta) = V(\theta)\cos\theta\,. \tag{2}$$

of V in the z-direction. The average of this z-component over the cap,

$$\frac{1}{A_{S_0}} \iint_{S_0} W(\theta) \sin\theta \, d\theta \, d\varphi \ , \quad A_{S_0} = 4\pi R^2 \sin^2(\theta_0/2) \ , \tag{3}$$

with A_{S_0} the area of the cap, is denoted by w_0. The time-independent part $p(r,\theta)$ of the pressure due to a harmonic excitation of the flexible membrane with z-component W of the velocity distribution is given by

$$p(r,\theta) = -i\rho_0 c \sum_{n=0}^{\infty} W_n \, P_n(\cos\theta) \, \frac{h_n^{(2)}(kr)}{h_n^{(2)'}(kR)} \ , \tag{4}$$

see [11, Ch. 7] or [19, Ch. 19]. Here ρ_0 is the density of the medium, c is the speed of sound in the medium, $k = \omega/c$ is the wave number with ω the radial frequency of the applied excitation, and $r \geq R$, $0 \leq \theta \leq \pi$ (the azimuthal variable φ is absent due to the assumption of axisymetric profiles). Furthermore, P_n is the Legendre polynomial of degree n [24], the coefficients W_n are given by

$$W_n = (n+1/2) \int_0^{\pi} W(\theta) P_n(\cos\theta) \sin\theta \, d\theta \ , \quad n = 0, 1, \cdots \ , \tag{5}$$

and $h_n^{(2)}$ and $h_n^{(2)'}$ are the spherical Hankel function and its derivative of order $n = 0, 1, \cdots$, [24, Ch. 10].

The case that $W = w_0$ is constant on the cap has been treated in [18, Part III, Sec. 6], [11, p. 343] and [19, Sec. 20.5] with the result that

$$W_n = \frac{1}{2} w_0 (P_{n-1}(\cos\theta_0) - P_{n+1}(\cos\theta_0)) \ . \tag{6}$$

The pressure p is then obtained by inserting these W_n into the right-hand-side of Eq. (4). Similarly, the case that $V = v_0$ is constant on S_0 has been treated in [19, Sec. 20.6], with the result that

$$\begin{aligned} W_n = \tfrac{1}{2} v_0 \{ & \tfrac{n+1}{2n+3} (P_n(\cos\theta_0) - P_{n+2}(\cos\theta_0)) + \\ & \tfrac{n}{2n-1} (P_{n-2}(\cos\theta_0) - P_n(\cos\theta_0)) \} \ . \end{aligned} \tag{7}$$

In Eqs. (6) and (7) the definition $P_{-n-1} = P_n$, $n = 0, 1, \cdots$, has been used to deal with the case $n = 0$ in Eq. (6) and the cases $n = 0, 1$ in Eq. (7). In [23, Eq. (20)], a formula for the expansion coefficients W_n in terms of expansion coefficients of the profile W with respect to orthogonal functions on the cap is given. This formula is instrumental in solving the inverse problem of estimating the W from pressure data measured around the sphere. However, for the present goals, that can be achieved by forward computation, this is not needed.

In Fig. 2, taken from [23, Fig. 2] the resemblance is shown between the polar plots of: a real driver in a rectangular cabinet (Fig. 2-a), a rigid piston in an infinite baffle (Fig. 2-b), and a rigid spherical cap in a rigid sphere (Fig. 2-c) using Eqs. (4) and (7). The driver (vifa MG10SD09-08, $a = 3.2$ cm) was mounted

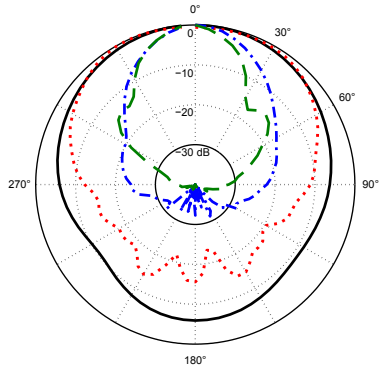

(a)

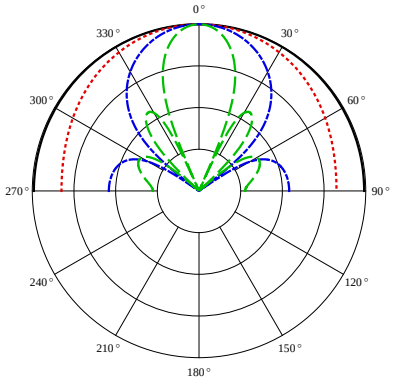

(b)

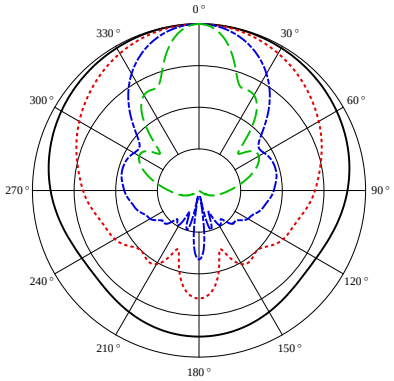

(c)

Figure 2: Polar plots of the SPL (10 dB/div.), f= 1 kHz (solid curve), 4 kHz (dotted curve), 8 kHz (dashed-dotted curve), and 16 kHz (dashed curve), corresponding for $c = 340$ m/s and $a = 3.2$ cm to ka values: 0.591, 2.365, 4.731, 9.462. All curves are normalized such that the SPL is 0 dB at θ=0. (a) Loudspeaker radius $a = 3.2$ cm, measuring distance $r = 1$ m) in rectangular cabinet, (b) Rigid piston ($a = 3.2$ cm) in infinite baffle, (c) Rigid spherical cap (aperture $\theta_0 = \pi/8$, sphere radius $R = 8.2$ cm, $r = 1$ m, corresponding to kR values: 1.5154, 6.0614, 12.1229, 24.2457) using Eqs. (4) and (7), constant velocity $V = v_0 = 1$ m/s. The parameters a, R, and θ_0 are such that the area of the piston and the cap are equal.

in a square side of a rectangular cabinet with dimensions 13x13x18.6 cm and measured on a turntable in an anechoic room at 1 m distance.

The area A_{S_0} of the spherical cap is given in Eq. (3). If this area is chosen to be equal to the area of the flat piston (a disk with radius a), there follows

$$a = 2R\sin(\theta_0/2). \tag{8}$$

The parameters used for Fig. 2, $a = 3.2$ cm, $\theta_0 = \pi/8$ and $R = 8.2$ cm, are such that the area of the piston and the cap are equal, while the sphere and the cabinet have comparable volumes (2.3 and 3.1 l, respectively). If R were chosen such that the sphere and cabinet have equal volume, the polar plot corresponding to the spherical cap model is hardly different from the one in Fig. 2-c, with deviations of about 1 dB or less, see [23, Fig. 2-c,d]. Apparently, the actual value of the volume is of modest influence. It is hard to give strict bounds to deviations of the actual size, but as a rule of thumb one can choose the volume of the sphere the same as that for the real cambinet, and the area of the cap the same as that of the driver. To gain more insight in this matter we keep R fixed and change the cap area by changing the aperture θ_0. To illustrate that the influence can be significant, polar plots are shown in Fig. 3 for constant $V = v_0 = 1$ m/s, using Eqs. (4) and (7). Figure 3 clearly shows that for increasing aperture angle θ_0 until, say, $\theta_0 = \pi/2$, the radiation becomes more directive.

In the limit case $\theta_0 = \pi$ there is only one non-zero W_n in Eqs. (6) and (7), viz. $W_n = \delta_{0n}$ for constant W and $W_n = \delta_{1n}$ for constant V, respectively (δ: Kronecker's delta). In the case of constant W this is a non-directive pulsating sphere. In the case of constant V there holds

$$p(r,\theta) = -i\rho_0 c\, v_0\, \cos\theta \frac{h_1^{(2)}(kr)}{h_1^{(2)'}(kR)}\ . \tag{9}$$

The latter case is discussed in Ref. [13, Sec. 4.-2] as the transversely oscillating rigid sphere. It is readily seen that $p(r,\theta)/p(r,0) = \cos\theta$ as is plotted in Fig. 4. Finally, consider the case of a simple source with a δ-mass b at the point $(0, 0, z = R)$. This can be obtained by taking $W(\theta) = w_0 = b/A_{S_0} \quad 0 \le \theta \le \theta_0$, and letting θ_0 decrease to 0. Since $P_n(1) = 1$ for all n, Eq. (5) gives $W_n = (2n+1)b$ for all n as θ_0 goes to 0, and there results

$$p(r,\theta) = -i\rho_0 c\, b \sum_{n=0}^{\infty}(2n+1)P_n(\cos\theta)\frac{h_n^{(2)}(kr)}{h_n^{(2)'}(kR)}\ . \tag{10}$$

This case is illustrated in [23, Fig. 3] from which it is apparent that the response at $\theta = 0$ and $\theta = \pi$ are of the same order of magnitude, especially at low frequencies. This is discussed further in Sec. 3.2 in connection with the acoustic center.

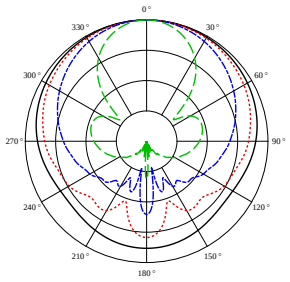

(a) $\theta_0 = \pi/16$

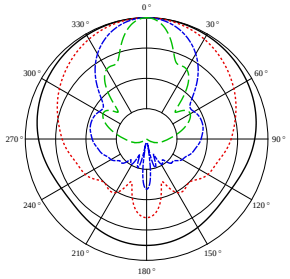

(b) $\theta_0 = 2\pi/16$

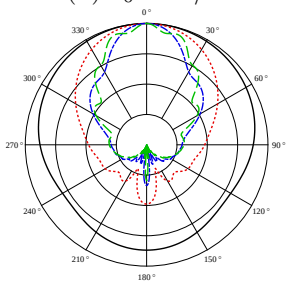

(c) $\theta_0 = 3\pi/16$

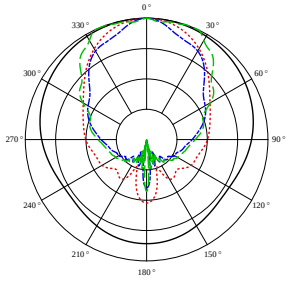

(d) $\theta_0 = 4\pi/16$

Figure 3: Polar plots of the SPL (10 dB/div.), f= 1 kHz (solid curve), 4 kHz (dotted curve), 8 kHz (dashed-dotted curve), and 16 kHz (dashed curve), Rigid spherical cap for various aperture θ_0, (sphere radius $R = 8.2$ cm, $r = 1$ m) using Eqs. (4) and (7), constant velocity $V = v_0 = 1$ m/s. All curves are normalized such that the SPL is 0 dB at θ=0.

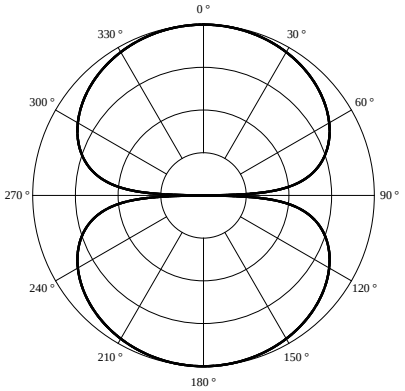

Figure 4: Polar plot for a sphere ($\theta_0 = \pi$) moving with constant velocity $V = v_0$ = 1 m/s in the z-direction, using Eqs. (4) and (7). In this case $W_1 = 1$, W_n is equal to zero for all values $n \neq 1$.

2 Comparison for baffle-step responses

At low frequencies the baffle of a loudspeaker is small compared to its wavelength and radiates due to diffraction effects in the full space (4π-field). At those low frequencies the radiator does not benefit from the baffle in terms of gain. At high frequencies the loudspeaker benefits from the baffle which yields a gain of 6 dB. This transition is the well-known baffle step. The center frequency of this transition depends on the size of the baffle. Olson [25] has documented this for twelve different loudspeaker enclosures, including the sphere, cylinder, and rectangular parallelepiped. All those twelve enclosures share the common feature of increasing gain by about 6 dB when the frequency is increased from low to high. The exact shape of this step depends on the particular enclosure. For spheres the transition is smoothest, while for other shapes undulations are manifest, in particular for cabinets with sharp-edged boundaries. In Fig. 5-a the baffle step is shown for a polar cap ($\theta_0 = \pi/8$, constant velocity $V = v_0 = 1$ m/s) on a sphere of radius R=0.082 m using Eqs. (4) and (7), for different observation angles $\theta = 0$ (solid curve), $\theta = \pi/9$ (dotted curve), $\theta = 2\pi/9$ (dashed-dotted curve), and $\theta = 3\pi/9$ (dashed curve). Compare the curves of Fig. 5-a with the measurements using the experimental loudspeaker (Fig. 5-b) discussed in Sec. 1 and that of a rigid piston in an infinite baffle (Fig. 5-c), using [12, 13, 14]

$$p_i(\theta)/p_i(\theta = 0) = J_1(ka\sin(\theta))/(ka\sin(\theta)) \tag{11}$$

for the normalized pressure. It appears that there is a good resemblance between the measured frequency response of the experimental loudspeaker. The undulations, e.g., for $\theta = 3\pi/9$ (dashed curve) at 7.4, 10, and 13.4 kHz correspond well. Although these undulations are often attributed to the non-rigid cone movement of the driver itself, our pictures show that it is mainly a diffraction effect. Furthermore, it can be observed that even on-axis ($\theta = 0$) there

is a gradual decrease of SPL at frequencies above about 10 kHz. It can be shown from the asymptotics of the spherical Hankel functions that for $\theta = 0$, $k \to \infty$, and $r \gg R$, the sound pressure $p(r, \theta)$ decays at least as $\mathrm{O}(k^{-1/3})$. This is in contrast with a flat piston in an infinite baffle (Fig. 5-c). There, the on-axis pressure does not decay, and the baffle step is absent. This is discussed further at the end of Sec. 3.2. Although it is highly speculative, and should be validated for different drivers and cabinets, one might expect that the ratio of the pressure of the cap using Eqs. (4), (7), and that of the pressure for the piston in an infinite baffle using Eq. (11) can assist in interpreting published loudspeaker response curves which are measured under standardized (infinite baffle) conditions. For typical loudspeakers at low frequencies the loss is theoretically 6 dB, but is counteracted by room placement - a range of 3 to 6 dB is usually allowed. At sufficiently high frequencies the piston does not benefit from the baffle because it is highly directional. Finally, the tests were made using a high-quality 3.5-inch loudspeaker. In such a unit, the first cone breakup mode usually occurs around 10 kHz. However the present one does not exhibit a clear breakup mode, because it is very well damped. This was verified with a PolyTec PSV-300-H scanning vibrometer with an OFV-056 laser head.

3 Comparison for power and directivity

3.1 Sound power

The sound power is meaningful in various respects. Firstly, it is used in efficiency calculations which we do not consider here. Secondly, it is important regarding sound radiation. Different loudspeakers may share a common, rather flat, on-axis SPL-response, while their off axis-responses differ considerably. Therefore we consider the power response as important. We restrict ourselves to axisymmetric drivers and we do not discuss horn loudspeakers. The power is defined as the intensity pv^* integrated over the sphere S_r of radius $r \geq R$,

$$P = \int_{S_r} pv^* dS_r \ , \tag{12}$$

where p and v are the pressure and velocity at an arbitrary point on the sphere S_r. Using Eq. (4) for the pressure and

$$v = \frac{-1}{ik\rho_0 c} \frac{\partial p}{\partial \underline{n}} \tag{13}$$

we get

$$v(r, \theta, \varphi) = \sum_{n=0}^{\infty} W_n \, P_n(\cos\theta) \, \frac{h_n^{(2)'}(kr)}{h_n^{(2)'}(kR)} \ . \tag{14}$$

By the orthogonality of the Legendre polynomials it follows that

$$\begin{aligned} P = \ & \textstyle\int_{S_r} pv^* dS_r = 2\pi \int_0^{\pi} p(r,\theta) v^*(r,\theta) r^2 \sin\theta d\theta = \\ & -i\rho_0 c \textstyle\sum_{n=0}^{\infty} \frac{|W_n|^2}{n+1/2} \, \frac{2\pi r^2 h_n^{(2)}(kr) (h_n^{(2)'}(kr))^*}{|h_n^{(2)'}(kR)|^2} \ . \end{aligned} \tag{15}$$

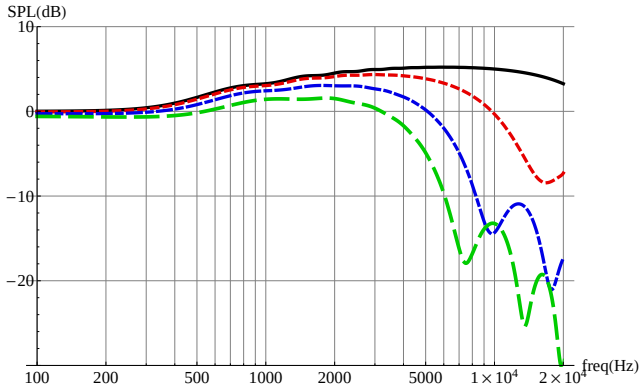

(a)

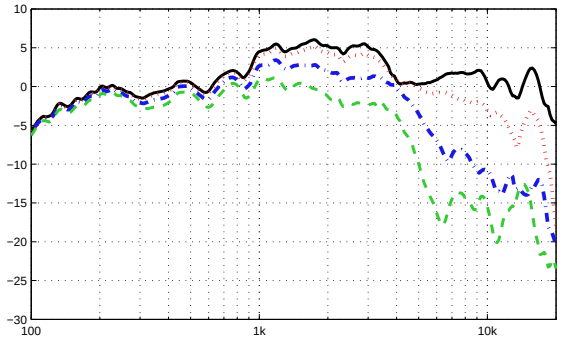

(b)

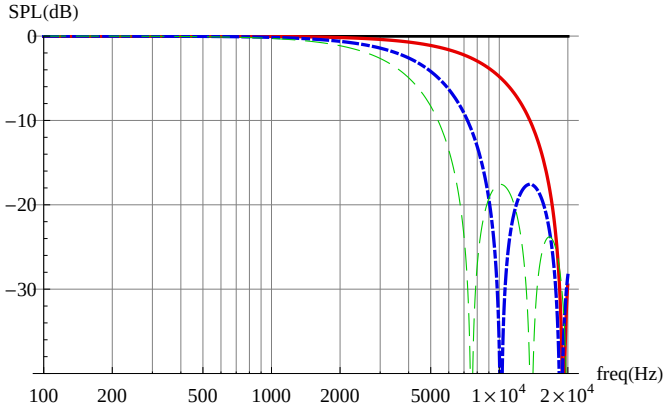

(c)

Figure 5: Frequency responses for $\theta = 0$ (solid curve), $\theta = \pi/9$ (dotted curve), $\theta = 2\pi/9$ (dashed-dotted curve), and $\theta = 3\pi/9$ (dashed curve). (a) Baffle step of a polar cap ($\theta_0 = \pi/8$) on a sphere of radius R =0.082 m, at distance r = 1 m, using Eqs. (4), (7) (constant velocity $V = v_0 = 1$ m/s). All curves are normalized such that the SPL is 0 dB at 100 Hz. (b) Frequency response of a driver (same as Fig. 2-a, $a = 3.2$ cm) mounted in a square side of a rectangular cabinet with dimensions 13x13x18.6 cm. The loudspeaker was measured in an anechoic room at 1 m distance. The on-axis response was normalized to 0 dB at 200 Hz, the other curves were normalized by the same amount. (c) Response of a rigid piston (a=3.2 cm) in a infinite baffle in the far field. All curves are normalized such that the SPL is 0 dB at 100 Hz.

Using Ref. [24], Eq. 10.1.6,

$$\mathcal{W}\{j_n(z), y_n(z)\} = j_n(z)y_n'(z) - j_n'(z)y_n(z) = \frac{1}{z^2}, \tag{16}$$

where $\mathcal{W}$ in Eq. (16) denotes the Wronskian, we get

$$\Re[P] = \frac{2\pi\rho_0 c}{k^2} \sum_{n=0}^{\infty} \frac{|W_n|^2}{(n+1/2)|h_n^{(2)'}(kR)|^2} \ . \tag{17}$$

Note that Eq. (17) has been derived without using any (near-field or far-field) approximation. The real part of the acoustical power is independent of r, which is in accordance with the conservation of power law. For low frequencies Eq. (17) is approximated as

$$\Re[P] = 4\pi\rho_0 c W_0^2 k^2 R^4 \ . \tag{18}$$

To illustrate Eq. (17), the normalized power $\frac{\Re[P]}{2\pi\rho_0 c v_0^2 R^2}$ is plotted in Fig. 6, where a cap with various apertures, $\theta_0 = 5\pi/32$ (solid curve), $\theta_0 = \pi/8$ (dotted curve), and $\theta_0 = \pi/10$ (dashed-dotted curve) is moving with a constant velocity $V = v_0$=1 m/s (using Eq. (7)).

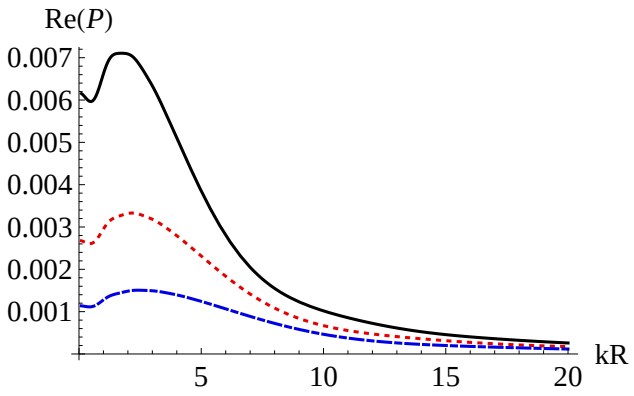

Figure 6: The power $\frac{\Re[P]}{2\pi\rho_0 c v_0^2 R^2}$ of a rigid spherical cap moving with a constant velocity ($V = v_0 = 1$ m/s) and various apertures, $\theta_0 = 5\pi/32$ (solid curve), $\theta_0 = \pi/8$ (dotted curve), and $\theta_0 = \pi/10$ (dashed-dotted curve), sphere radius $R = 8.2$ cm using Eqs. (7) and (17).

Next, we compare the calculated power with the power measured in a reverberation room using the experimental loudspeaker discussed in Sec. 1. Here we assumed the pole cap moving not with a constant velocity but with with a constant acceleration ($V' = ikcV$)—corresponding with a frequency independent current of a constant amplitude through the loudspeaker. Figure 7 shows plots of the calculated power for a rigid spherical cap moving with a constant

acceleration and various apertures, $\theta_0 = 5\pi/32$ (solid curve), $\theta_0 = \pi/8$ (dotted curve), and $\theta_0 = \pi/10$ (dashed-dotted curve), together with the power obtained from the measured loudspeaker (dashed-irregular curve). It appears that the

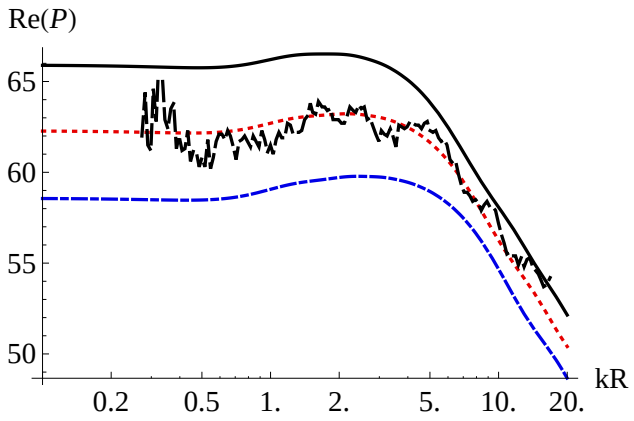

Figure 7: The power $\frac{\Re[P]c}{2\pi\rho_0 a_0^2 R^4}$ [dB] vs. kR (log. axis) of a rigid spherical cap moving with a constant acceleration ($V' = ikcV$) and various apertures, $\theta_0 = 5\pi/32$ (solid curve), $\theta_0 = \pi/8$ (dotted curve), and $\theta_0 = \pi/10$ (dashed-dotted curve), sphere radius $R = 8.2$ cm using Eqs. (7) and (17), together with the power from the measured loudspeaker (dashed-irregular curve). The logarithmic horizontal axis runs from kR=0.1–20, corresponding to a frequency range from 66 Hz–13.2 kHz.

calculated power for $\theta_0 = \pi/8$ (dotted curve) and the power from the measured loudspeaker (dashed-irregular curve) are quite similar, while there was no special effort done to obtain a best fit. A slightly larger aperture than the 'round' value $\theta_0 = \pi/8$, which we use in many examples in the paper, would have resulted in a better fit. The low-frequency behavior of Fig. 7 follows directly by multiplying Eq. (18) with $1/(kc)^2$ because of the constant acceleration of the cap.

3.2 Directivity

The far-field pressure can be calculated by substituting the asymptotic value [24, Ch. 10]

$$h_n^{(2)}(kr) \approx i^{n+1} \frac{\mathrm{e}^{-ikr}}{kr} \tag{19}$$

in Eq. (4), which leads to

$$p(r,\theta) \approx \rho_0 c \frac{\mathrm{e}^{-ikr}}{kr} \sum_{n=0}^{\infty} \frac{i^n W_n}{h_n^{(2)'}(kR)} P_n(\cos\theta) \; . \tag{20}$$

In Kinsler et al. [12, Sec. 8.9], the far-field relation is written as

$$p(r,\theta,\varphi) = p_{ax}(r)H(\theta,\varphi), \tag{21}$$

in which $p_{ax}(r)$ is the pressure at $\theta = 0$, and $H(\theta,\varphi)$ is dimensionless with $H(0,0)$=1. Since there is no φ dependence, we delete it. This leads to

$$p_{ax}(r) = \rho_0 c \frac{\mathrm{e}^{-ikr}}{kr} \sum_{n=0}^{\infty} \frac{i^n W_n}{h_n^{(2)'}(kR)} \ , \tag{22}$$

and

$$H(\theta) = \frac{p(r,\theta)}{p_{ax}(r)} = \frac{\sum_{n=0}^{\infty} \frac{i^n W_n}{h_n^{(2)'}(kR)} P_n(\cos\theta)}{\sum_{n=0}^{\infty} \frac{i^n W_n}{h_n^{(2)'}(kR)}}. \tag{23}$$

The total radiated power Π in the far field follows from Eq. (12) and the far-field relation $v = p/(\rho_0 c)$ as

$$\begin{aligned} \Pi = \ & \textstyle\int_{S_r} \frac{1}{\rho_0 c}|p|^2 dS_r = \\ & \textstyle\frac{1}{\rho_0 c}|p_{ax}(r)|^2 r^2 \int_0^{2\pi} \int_0^{\pi} |H(\theta)|^2 \sin\theta \, d\theta \, d\varphi \ . \end{aligned} \tag{24}$$

For a simple (non-directive) source at the origin to yield the same acoustical power on S_r, the pressure p_s should satisfy

$$\Pi = \frac{1}{\rho_0 c} 4\pi r^2 |p_s(r)|^2 \ . \tag{25}$$

Therefore, the directivity defined as

$$D = |p_{ax}(r)|^2 / |p_s(r)|^2 \ , \tag{26}$$

follows from Eqs. (23)–(25), using the orthogonality of the Legendre polynomials, as

$$D = \frac{2|\sum_{n=0}^{\infty} \frac{i^{n+1} W_n}{h_n^{(2)'}(kR)}|^2}{\sum_{n=0}^{\infty} \frac{|W_n|^2}{(n+1/2)|h_n^{(2)'}(kR)|^2}} \ . \tag{27}$$

The directivity index $DI = 10 \log_{10} D$ [dB] vs. kR is plotted in Fig. 8 for a cap moving with constant velocity V. For comparison the directivity

$$D_{rp} = \frac{(ka)^2}{1 - J_1(2ka)/ka} \tag{28}$$

of a rigid piston in an infinite baffle [12] is plotted in Fig. 8 (with $ka = kR/2.5$, so that the $\pi/8$-cap and piston have the same area), as the light-long-dashed curve starting at 3 dB. At low frequencies the directivity D_{rp} is 3 dB because the piston is radiating in the 2π-field, while the caps are radiating in the 4π-field. At higher frequencies the curve almost coincides with the dotted curve which corresponds to the $\theta_0 = \pi/8$ cap.

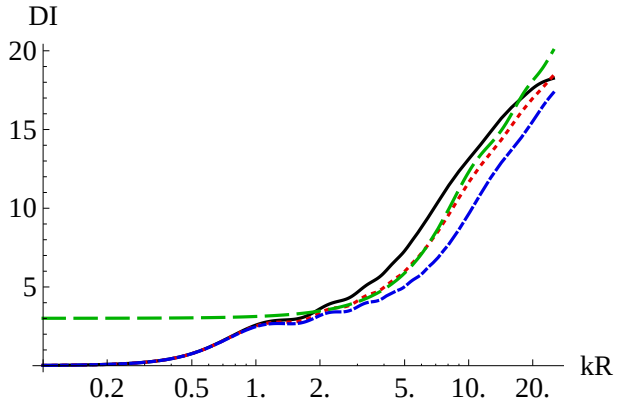

Figure 8: The directivity index $DI = 10\log_{10} D$ [dB] vs. kR (log. axis) of a rigid spherical cap with various apertures, $\theta_0 = 5\pi/32$ (solid curve), $\theta_0 = \pi/8$ (dotted curve), and $\theta_0 = \pi/10$ (dashed-dotted curve), moving with constant velocity V and sphere radius $R = 8.2$ cm using Eqs. (7) and (27). The light-long-dashed curve starting at 3 dB is the directivity for a rigid piston in an infinite baffle, using Eq. (28). The logarithmic horizontal axis runs from kR=0.1–25, corresponding to a frequency range from 66 Hz–16.5 kHz.

Now consider the case that $kR \to \infty$. Then using $h_n^{(2)'}(kR) \approx i^n \mathrm{e}^{-ikR}/kR$, it follows that D is approximated by

$$D \approx \frac{2|\sum_{n=0}^{\infty} W_n|^2}{\sum_{n=0}^{\infty} \frac{|W_n|^2}{(n+1/2)}} = \frac{2|W(\theta=0)|^2}{\int_0^{\pi} |W(\theta)|^2 \sin\theta d\theta}, \tag{29}$$

or, in words, by the ratio of $|W(\theta = 0)|^2$ and the average value of $|W(\theta)|^2$ over the sphere. Equations (27) and (29) show that the directivity—which is a typical far-field acoustical quantity—is fully determined in a simple manner by the velocity profile of the pole cap, which can be easily derived from measurements, e.g., with a laser-Doppler meter. This procedure is not elaborated here. A similar result was obtained for a flexible radiator in an infinite flat baffle [10]. In the flat baffle case the directivity increases with $(ka)^2$. For the cap case, there is indeed an initial increase with $(kR)^2$, but at very high frequencies, there is a decrease of the directivity. These high frequencies are in most cases out of the audio range, but may be of importance for ultrasonics. The deviation of the $(kR)^2$-behavior appears in Fig. 8 for θ_0 as low as $5\pi/32$ (solid curve). This effect may seem counterintuitive or even non-physical, however, the on-axis ($\theta = 0$) pressure decreases for high frequencies as well (see Fig. 5). This will decrease the numerator in Eq. (26) of the right-hand side of Eq. (26). This effect does not occur with a piston in an infinite baffle, which has a constant, non-decreasing on-axis sound pressure, but a narrowing beam width.

4 The acoustic center

The acoustic center of a reciprocal transducer can be defined as the point from which spherical waves seem to be diverging when the transducer is acting as a source. There are more definitions, however, see Ref. [26] for an overview and discussion. This concept is mainly used for microphones. Recently, the acoustic center was elaborated [27, 28] for normal sealed-box loudspeakers as a particular point that acts as the origin of the low-frequency radiation of the loudspeaker. At low frequencies, the radiation from such a loudspeaker becomes simpler as the wavelength of the sound becomes larger relative to the enclosure dimensions, and the system behaves externally as a simple source (point source). The difference from the origin to the true acoustic center is denoted as Δ. If $p(r,0)$ and $p(r,\pi)$ are the sound pressure in front and at the back of the source, respectively, then Δ follows from

$$\frac{|p(r,0)|}{r+\Delta} = \frac{|p(r,\pi)|}{r-\Delta}\ , \tag{30}$$

as

$$\Delta = r\frac{|q|-1}{|q|+1}, \tag{31}$$

where

$$q = p(r,0)/p(r,\pi). \tag{32}$$

The pole-cap model is used to calculate the function q via Eq. (4), see Fig. 9.

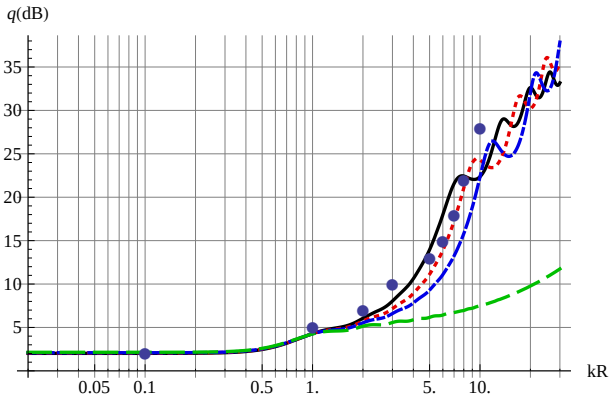

Figure 9: The function $20\log_{10}|q|$ [dB] vs. kR (log. axis) given by Eq. (32) of a rigid spherical cap with various apertures, $\theta_0 = 5\pi/32$ (solid curve), $\theta_0 = \pi/8$ (dotted curve), and $\theta_0 = \pi/10$ (dashed-dotted curve), using Eqs. (4) and (7), and a simple source on a sphere using Eq. (10) (dashed curve), moving with constant velocity V, all at $r = 1$ m and sphere radius $R = 8.2$ cm. The solid circles are from a real driver (same as Fig. 2-a, $a = 3.2$ cm) mounted in a square side of a rectangular cabinet. The logarithmic horizontal axis runs from kR=0.02–30, corresponding to a frequency range from 13 Hz–19.8 kHz.

Subsequently, this model is used to compute the acoustic center with Eq. (31). Assume that $kR \ll 1$ and $R/r \ll 1$, and also that W_n is real with W_n of at most the same order of magnitude as W_0. Then two terms of the series in Eq. (4) are sufficient, and using $P_n(1) = 1$ and $P_n(-1) = (-1)^n$, q can be written as

$$\begin{aligned} q \approx \quad & \Big(W_0 \, \tfrac{h_0^{(2)}(kr)}{h_0^{(2)'}(kR)} + W_1 \, \tfrac{h_1^{(2)}(kr)}{h_1^{(2)'}(kR)}\Big) \Big/ \\ & \Big(W_0 \, \tfrac{h_0^{(2)}(kr)}{h_0^{(2)'}(kR)} - W_1 \, \tfrac{h_1^{(2)}(kr)}{h_1^{(2)'}(kR)}\Big). \end{aligned} \tag{33}$$

Because $kR \ll 1$, the small argument approximation of the spherical Hankel functions

$$h_0^{(2)'}(z) \approx \frac{-i}{z^2}, \; h_1^{(2)'}(z) \approx \frac{-2i}{z^3}, \tag{34}$$

can be used, and together with the identity

$$\frac{h_1^{(2)}(kr)}{h_0^{(2)}(kr)} = \frac{1}{kr}(1 + ikr) \; , \tag{35}$$

we get

$$q \approx \Big(1 + \frac{W_1}{2W_0}(1 + ikr)\frac{R}{r}\Big) \Big/ \Big(1 - \frac{W_1}{2W_0}(1 + ikr)\frac{R}{r}\Big) \; . \tag{36}$$

By our assumptions we have $|\frac{W_1}{2W_0}(1 + ikr)\frac{R}{r}| \ll 1$ and so

$$q \approx 1 + \frac{W_1}{W_0}\frac{R}{r}(1 + ikr) \; . \tag{37}$$

Finally, assuming that $(kr)^2 \ll 2|\frac{W_0}{W_1}|\frac{r}{R}$, there holds

$$|q| \approx 1 + \frac{W_1}{W_0}\frac{R}{r} \; , \tag{38}$$

and if $\frac{W_1 R}{W_0 r} \ll 1$ there holds

$$\varphi_q = \arg q \approx \arctan \frac{W_1}{W_0}\frac{\omega R}{c} \; , \tag{39}$$

where it has been used that W_1/W_0 is real and $k = \omega/c$. Substitution of Eq. (38) into Eq. (31) results in

$$\Delta \approx \frac{R \, W_1}{2 \, W_0} \; . \tag{40}$$

Note that this result is real, independent of k and r, and only mild assumptions were used. The delay between the front and at the back of the source is equal to $\tau = d\varphi_q/d\omega$. Using Eqs. (39) and (40), and assuming $kR \ll \frac{W_0}{W_1}$ we get

$$\tau \approx \frac{2\Delta}{c} \; . \tag{41}$$

For the case W is constant the W_n follow from Eq. (6) resulting in

$$\Delta \approx \frac{3}{4} R(1 + \cos\theta_0) \; . \tag{42}$$

If $\theta_0 = \pi$ and W is constant, the radiator is a pulsating sphere, and has according to Eq. (42) its acoustical center at the origin. For the case V is constant the W_n follow from Eq. (7) resulting in

$$\Delta \approx R\big(\cos\theta_0 + \frac{1}{1 + \cos\theta_0}\big) \; . \tag{43}$$

If $\theta_0 = \pi$ and V is constant, the notion of acoustical center does not make sense, because of the notches in the polar plot at low frequencies, see Fig. 4. The absolute error in the approximation of Δ/R by Eq. (43) (for f=1 Hz, R=8.2 cm, r=100 m, and $0 \le \theta_0 \le \pi/2$) is $< 5\,10^{-7}$. Figure 9 shows that for a cap moving with constant velocity V that case the low-frequency asymptote is flat to about $kR = 0.4$ corresponding to 264 Hz. Hence the approximation of Δ/R by Eq. (43) is rather accurate up to this frequency. The relative acoustic center difference Δ/R vs. θ_0 is plotted in Fig. 10 for W is constant (solid curve) and V is constant (dotted curve), using Eqs. (42) and (43), respectively. Note that Δ/R=3/2 for $\theta_0 = 0$ in both cases that V and W are constant. This agrees with what would be given by the simple source on a sphere, see Eq. (10). We have W_0=1 and W_1=3, and by Eq. (40) we obtain Δ/R=3/2. This is for low frequencies also shown in Ref. [26, Fig. 3, Eqs. 18–19]. Further, it appears that for modest apertures, say $\theta_0 \le 0.5$ the difference between the right-hand sides of Eqs. (42) and (43) is very small and is of order θ_0^4. From this we may conclude that—at low frequencies ($kR \le 0.4$)—the acoustic center for a loudspeaker lies about 0–0.5 R in front of the loudspeaker, where R is the radius in the case of a spherical cabinet, or some other dimensional measure of the cabinet. At higher frequencies the acoustic center shifts further away from the loudspeaker. For example between kR=1 (660 Hz) and kR=2 (1.32 kHz), q is about 5 dB (see Fig. 9) corresponding (using Eq. (31)) to $\Delta = 3.4R = 28$ cm.

The polar response $|p(r,\theta)/p(r,0)|$ at low frequencies can be computed in a similar way as q in Eq. (36). The minus sign in the denominator at the right-hand side of Eq. (36) is due to $P_1(\cos\pi) = -1$. Using now $P_1(\cos\theta) = \cos\theta$ and interchanging the numerator and denominator of Eq. (36) yields

$$\begin{aligned} &\frac{p(r,\theta)}{p(r,0)} \approx \\ &\quad \Big(1 + \frac{W_1}{2W_0}(1 + ikr)\frac{R}{r}\cos\theta\Big)\Big/\Big(1 + \frac{W_1}{2W_0}(1 + ikr)\frac{R}{r}\Big) \; . \end{aligned} \tag{44}$$

Assuming that $(kr)^2 \ll 2|\frac{W_0}{W_1}|\frac{r}{R}$, Eq. (44) can be approximated by

$$\Big|\frac{p(r,\theta)}{p(r,0)}\Big| \approx 1 + (\cos\theta - 1)\frac{W_1}{2W_0}\,\frac{R}{r}. \tag{45}$$

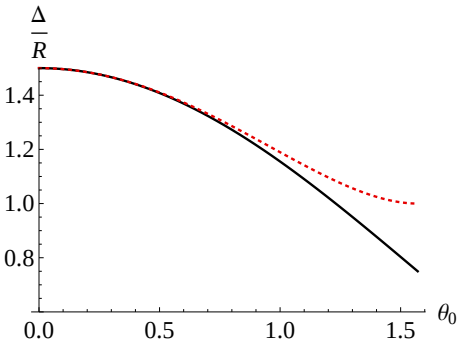

Figure 10: The relative acoustic center difference Δ/R vs. θ_0 using Eq. (42) for W is constant (solid curve) and using Eq. (43) for $V = v_0 = 1$ m/s is constant (dotted curve).

Equation (45) clearly shows that the deviation from omni-directional radiation is proportional to the ratios $W_1/2W_0$ and R/r, while it is independent of the frequency for low frequencies. For fixed $W_1/2W_0$ and R/r the polar pattern is not truly omni-directional at low frequencies. This is because the acoustic center does not coincide with the origin in general .

5 Conclusions and outlook

The polar plot of a rigid spherical cap on a rigid sphere has been shown to be quite similar to that of a real loudspeaker (see Fig. 2), and is useful in the full 4π-field. It thus outperforms the more conventional model in which the loudspeaker is modeled as a rigid piston in an infinite baffle. The cap model can be used to predict, besides polar plots, various other acoustical quantities of a loudspeaker. These quantities include the sound pressure, baffle-step response, sound power, directivity, and the acoustic center. The baffle-step response of the model is rather similar to that of a loudspeaker (see Fig. 5). The sound power predicted by the model is very similar to that of a loudspeaker measured in a reverberation room (see Fig. 7). The directivity D given by the model is approximated as the ratio of $|W(\theta = 0)|^2$ and the average value of $|W(\theta)|^2$ over the sphere (see Eq. (29)). The ratio of the sound pressure in front and at the back of the loudspeaker, which is associated with the acoustic center, is for the loudspeaker very similar as given by the model (see Fig. 9). At low frequencies the acoustic center for a loudspeaker lies about 0–0.5 times the sphere radius in front of the loudspeaker (see Fig. 10). At higher frequencies the acoustic center shifts further away from the loudspeaker. All results are obtained using only one loudspeaker, however. The value of this model for other drivers in other cabinets should be tested in order to derive bounds of the applicability of the model. This is work to be done in the future.

Acknowledgments

The authors dedicate this paper to Mrs. Doortje Aarts-Ultee who passed away at age 53 on August 6, 2009 while this paper was taking shape. The authors wish to thank Okke Ouweltjes for assisting in the loudspeaker measurements and making the plot for Fig. 2-a, and the reviewers for pertinent suggestions which made the paper considerably more readable.

References

[1] J.W.S. Rayleigh. *The Theory of Sound, Vol. 2, 1896.* (reprinted by Dover, New York, 1945).

[2] L.V. King. On the acoustic radiation field of the piezo-electric oscillator and the effect of viscosity on transmission. *Can. J. Res.*, 11:135–155, 1934.

[3] M. Greenspan. Piston radiator: Some extensions of the theory. *J. Acoust. Soc. Am.*, 65(3):608–621, March 1979.

[4] G.R. Harris. Review of transient field theory for a baffled planar piston. *J. Acoust. Soc. Am.*, 70(1):10–20, July 1981.

[5] T. Hasegawa, N. Inoue, and K. Matsuzawa. A new rigorous expansion for the velocity potential of a circular piston source. *J. Acoust. Soc. Am.*, 74(3):1044–1047, Sept. 1983.

[6] D.A. Hutchins, H.D. Mair, P.A. Puhach, and A.J. Osei. Continuous-wave pressure fields of ultrasonic transducers. *J. Acoust. Soc. Am.*, 80(1):1–12, July 1986.

[7] R. C. Wittmann, and A. D. Yaghjian. Spherical-wave expansions of piston-radiator fields. *J. Acoust. Soc. Am.*, 90(3):1647–1655, Sept. 1991.

[8] T.J. Mellow. On the sound field of a resilient disk in an infinite baffle. *J. Acoust. Soc. Am.*, 120(1):90–101, July 2006.

[9] R.M. Aarts, and A.J.E.M. Janssen. On-axis and far-field sound radiation from resilient flat and dome-shaped radiators. *J. Acoust. Soc. Am.*, 125(3):1444–1455, March 2009.

[10] R.M. Aarts, and A.J.E.M. Janssen. Sound radiation quantities arising from a resilient circular radiator. *J. Acoust. Soc. Am.*, 126(4):1776–1787, Oct. 2009.

[11] P.M. Morse, and K.U. Ingard. *Theoretical acoustics.* McGraw-Hill Book Company, New York, 1968.

[12] L.E. Kinsler, A.R. Frey, A.B. Coppens, and J.V. Sanders. *Fundamentals of Acoustics.* Wiley, New York, 1982.

[13] A.D. Pierce. *Acoustics, An Introduction to Its Physical Principles and Applications*. Acoustical Society of America through the American Institue of Physics, 1989.

[14] D.T. Blackstock. *Fundamentals of physical Acoustics*. John Wiley & Sons, New York, 2000.

[15] H. Suzuki and J. Tichy. Sound radiation from convex and concave domes in an infinite baffle. *J. Acoust. Soc. Am.*, 69(1):41–49, Jan. 1981.

[16] H. Suzuki and J. Tichy. Radiation and diffraction effects of convex and concave domes. *J. Audio Eng. Soc.*, 29(12):873–881, Dec. 1981.

[17] P.M. Morse, and H. Feshbach. *Methods of theoretical physics*. McGraw-Hill, 1953.

[18] H. Stenzel, and O. Brosze. *Guide to computation of sound phenomena (published in German as Leitfaden zur Berechnung von Schallvorgängen), 2nd ed.* Springer-Verlag, Berlin, 1958.

[19] E. Skudrzyk. *The Foundations of Acoustics*. Springer-Verlag, New York, 1971, ASA-reprint 2008.

[20] R. New, R.I. Becker, and P. Wilhelmij. A limiting form for the nearfield of the baffled piston. *J. Acoust. Soc. Am.*, 70(5):1518–1526, Nov. 1981.

[21] Peter H. Rogers, and A.O. Williams, Jr. Acoustic field of circular plane piston in limits of short wavelength or large radius. *J. Acoust. Soc. Am.*, 52(3B):865–870, Sept. 1972.

[22] T. Hélie, and X. Rodet. Radiation of a pulsating portion of a sphere: Application to horn radiation. *Acta Acustica united with Acustica*, 89(4), 565–577, July/Aug. 2003

[23] R.M. Aarts, and A.J.E.M. Janssen. Sound radiation from a resilient spherical cap on a rigid sphere. *J. Acoust. Soc. Am.*, 127(4), 2262–2273, April 2010.

[24] M. Abramowitz, and I.A. Stegun. *Handbook of Mathematical Functions*. Dover, New York, 1972.

[25] Harry F. Olson. Direct radiator loudspeaker enclosures. *J. Audio Eng. Soc.* 17(1), 22–29, Jan. 1969.

[26] Finn Jacobsen, Salvador Barrera Figueroa, and Knud Rasmussen. A note on the concept of acoustic center. *J. Acoust. Soc. Am.*, 115(4):1468–1473, April 2004.

[27] John Vanderkooy. The acoustic center: A new concept for loudspeakers at low frequencies. *AES* Convention paper 6912 presented at the 121$^{\text{th}}$ Convention, San Francisco, Oct. 5–8, 2006.

[28] John Vanderkooy. The low-frequency acoustic center: measurement, theory, and application. *AES* Convention paper 7992 presented at the 128$^{\text{th}}$ Convention, London, May 22–25, 2010.

List of Figures